Turbulence spreading and transport scaling in global gyrokinetic particle simulations

Z. Lin
Department of Physics and Astronomy, University of California, Irvine, California 92697

T. S. Hahm
Princeton Plasma Physics Laboratory, Princeton University, P.O. Box 451, Princeton, New Jersey 08543

(Received 24 October 2003; accepted 12 December 2003)

An intriguing observation in magnetically confined plasma experiments and in global gyrokinetic particle simulations of toroidal ion temperature gradient turbulence is that the fluctuations are microscopic, while the resulting turbulent transport is not gyro-Bohm [Z. Lin *et al.*, Phys. Rev. Lett. **88**, 195004 (2002)]. A possible resolution to this puzzle is identified as turbulence spreading from the linearly active (unstable) region to the linearly inactive (stable) region. Large scale gyrokinetic simulations found that transport driven by microscopic fluctuations is diffusive and local, whereas the fluctuation intensity is determined by nonlocal effects. Fluctuations are found to spread from the linearly active region to the linearly inactive region. This turbulence spreading reduces the fluctuation intensity in the unstable region, especially for a smaller device size, and thus introduces a nonlocal dependence in the fluctuation intensity. The device size dependence of the fluctuation intensity, in turn, is responsible for the observed gradual transition from Bohm to gyro-Bohm transport scaling. © *2004 American Institute of Physics.* [DOI: 10.1063/1.1647136]

I. INTRODUCTION

An outstanding issue in turbulent transport in magnetically confined plasmas[1,2] is the device size scaling of the global energy confinement time, which enables extrapolations of turbulent transport properties from present-day tokamak experiments to larger fusion reactors. In the absence of a fundamental, first-principles turbulence theory, heuristic, mixing length rules are often utilized to estimate the size scaling of turbulent transport.[3,2] This approach invokes a random walk type of picture for diffusive processes using the scale length of turbulent eddies as the step size and the linear growth time of the instability as the step time. It predicts that Bohm-like transport scaling implies that the eddy size increases with the device size in the diffusive transport. On the other hand, if the eddy size is microscopic (scales with the gyroradius), the transport scaling is gyro-Bohm. However, dimensionless scaling studies on the DIII-D tokamak found[4] that the ion transport and energy confinement time exhibit Bohm-like behavior, while fluctuation characteristics are microscopic, which suggests a gyro-Bohm scaling for transport. A similar trend was observed in transport studies of the Joint European Torus (JET) tokamak[5] and a scan of power thresholds for the formation of internal transport barriers.[6]

This intriguing feature of the size scaling of fluctuations and transport has been critically examined[7] in our global gyrokinetic particle simulations of electrostatic ion temperature gradient (ITG) turbulence. Large scale simulations found, by varying the device size while keeping other dimensionless plasma parameters fixed, that the fluctuation scale length is microscopic in the presence of zonal flows, while the local transport coefficient exhibits a gradual transition from a Bohm-like scaling for device sizes corresponding to present-day experiments to a gyro-Bohm scaling for future larger devices. The device size where this transition occurs is much larger than that expected from linear theory based on profile variation of the pressure gradient. These findings show that extrapolations based on empirical scalings or mixing length rules, or local simulations, can be unreliable, and that full device nonlinear simulations can play a key role in complementing and eventually replacing extrapolation methods, by directly addressing parameter regimes inaccessible through conventional analytic or experimental approaches.

In this article, we present results from gyrokinetic toroidal code (GTC) simulations which show that the key to reconciling the deviation from gyro-Bohm transport scaling with microscopic fluctuations is turbulence spreading from the linearly active (unstable) zone to the linearly inactive (stable) zone in the presence of radial variation of the pressure gradient. We found that fluctuations are microscopic, that the transport process is diffusive and local, whereas the fluctuation intensity is determined by nonlocal effects. Specifically, the spatial and temporal correlation functions, and the radial and poloidal spectra of density fluctuations are independent of the device size. The probability density functions (PDF) of fluctuations and heat fluxes decay exponentially. Test particle transport is diffusive, and the transport coefficient is proportional to the local intensity of fluctuations. On the other hand, fluctuations are found to spread from the linearly active region to the linearly inactive region. This turbulence spreading reduces the fluctuation intensity in the unstable region, especially for smaller device sizes, and thus introduces a nonlocal dependence in the fluctuation intensity. The device size dependence of fluctuation intensity, in turn, is responsible for the observed gradual transition from Bohm to gyro-Bohm transport scaling in the presence of microscopic fluctuations.

It is encouraging to note that our initial report of radial penetration of fluctuations from the unstable region to the stable region, and its relation to the transport scaling through the fluctuation intensity dependence of the thermal conductivity,[7,8] has stimulated the development of a number of independent dynamical theories for turbulence spreading. Key features of the simulation results have been reproduced in theoretical models for the turbulence spreading based on radial diffusion resulting from nonlinear mode coupling[9] or based on radial propagation of dispersive waves nonlinearly enhanced by drift wave-zonal flow interaction.[10] For example, these theories[9,10] have qualitatively confirmed GTC simulation results for the spreading distance, the device size for the Bohm to gyro-Bohm transition, and the dynamical process of radial envelope expansion. These theories also predict that, in the absence of avalanche-like, large transport events, the transport coefficients (which we shall call ''local results'') of the ITG turbulence should be determined by local plasma parameters in the large device limit (i.e., in the gyro-Bohm regime) via a local balance of linear growth with linear and nonlinear damping.[9]

In addressing the transport scaling, it is important to have a simulation approach which can treat various mesoscale phenomena,[11,12] including the turbulence spreading, self-consistently. It is worthwhile to note that the fundamental assumption of flux-tube simulations[13] is that these local results exist, and can be reproduced in flux-tube simulations with radially periodic boundary conditions when the turbulence correlation length is much shorter than the simulation box size. The ability of a global code to simulate turbulence in a large device, where the gyro-Bohm transport scaling can be produced from first-principles calculations, can provide a theoretical foundation for testing the fundamental assumption of flux-tube simulations, i.e., the flux-tube simulation results as proxies for the local results.

In retrospect, the size scaling of turbulent transport has been a subject for intense studies, and continuing debates, in magnetic fusion research. Our GTC simulation results of a gradual transition from Bohm to gyro-Bohm scaling were criticized by Candy and Waltz in a series of publications[8,14] based on sometimes evolving and self-contradictory, ''*a priori* expectations'' and simulation results of gyro-Bohm scaling from the continuum code GYRO. However, a drastic reversion of results from GYRO simulations[15] with ''more care and details'' has recently confirmed the earlier GTC simulation results.[7,8]

In Sec. II we discuss transport scaling measured from GTC simulations of the toroidal ITG turbulence. In Sec. III we present fluctuation characteristics. Fluctuation spreading from the linearly active zone to the linearly inactive zone is discussed in Sec. IV. Conclusions are drawn in Sec. V.

II. TRANSPORT SCALING

Our present studies utilize a well benchmarked, massively parallel, full torus gyrokinetic toroidal code (GTC).[16] GTC employs magnetic coordinates[17,18] and a nonspectral Poisson solver[19] suitable for general geometry. The nonspectral Poisson solver allows realistic treatment of the equilibrium profile variation such as steep pressure gradients. Toroidal geometry is treated rigorously, e.g., the radial variations of safety factor, magnetic shear, and trapped particle fraction are retained in global simulations. Both linear and nonlinear wave–particle resonances, and finite Larmor radius effects are treated in gyrokinetic particle simulations.[20–22] Magnetic coordinates provide the most general coordinate system for any magnetic configuration possessing nested surfaces. The property of straight field lines in magnetic coordinates is desirable for describing the microinstabilities with field-aligned mode structures and for efficiently integrating the electron and ion orbits. The guiding center equations of motion[18] can be derived from a Hamiltonian formulation which conserves phase space volume and is best for integrating particle orbits for a long period. The fact that only scalar field quantities are needed to calculate the guiding center orbit in this framework is most suitable for the general geometry equilibrium.

A challenge for full torus turbulence simulations is that the computational cost grows rapidly with the device size, i.e., the number of computations, N_c, has a cubic dependence on the device size, $N_c \sim (a/\rho_i)^3$, where a is the tokamak minor radius and ρ_i is the ion gyroradius. The large device simulations reported in this paper only became feasible with the implementation of an efficient global field-aligned mesh using magnetic coordinates to take advantage of the quasi-2D structure of toroidal drift wave eigenmodes. The global field-aligned mesh, contrary to that employed in flux-tube codes, provides the highest possible computational efficiency without any simplification in terms of physics models or simulation geometry. As a result, the GTC code has a unique feature that the number of computations has a quadratic dependence on the device size, i.e., $N_c \sim (a/\rho_i)^2$. This reduces computational requirements by two orders of magnitude for reactor scale ITG simulations. A detailed description of the global field-aligned mesh will be published in a separate paper.

Our studies use representative parameters of DIII-D tokamak H-mode core plasmas[13] which have a peak ion temperature gradient at $r=0.5a$ with the following local parameters: $R_0/L_T=6.9$, $R_0/L_n=2.2$, $q=1.4$, $\hat{s}\equiv(r/q)(dq/dr)=0.78$, $T_e/T_i=1$, and $a/R_0=0.36$. Here R_0 is the major radius, a is the minor radius, L_T and L_n are the temperature and density gradient scale lengths, respectively, T_i and T_e are the ion and electron temperatures, and q is the safety factor. These parameters give rise to a strong ITG instability with a linear threshold of $(R_0/L_T)^{\mathrm{crit}}=4.0$. Our global simulations used fixed boundary conditions with electrostatic potential $\delta\phi=0$ enforced at $r<0.1a$ and $r>0.9a$. The simplified physics model includes a parabolic profile of $q=0.854+2.184(r/a)^2$, a temperature gradient profile of $\exp\{-[(r-0.5a)/0.28a]^6\}$ (shown in the lower panel of Fig. 1), a circular cross section, no impurities, and electrostatic fluctuations with an adiabatic electron response. Externally driven plasma flows and collisions are not treated in these simulations. The marker temperature and density are assumed constant to focus on the simplest problem of the radial variation of the pressure gradient (i.e., ω^* shear effects, ω^* is the diamagnetic frequency). The computational mesh

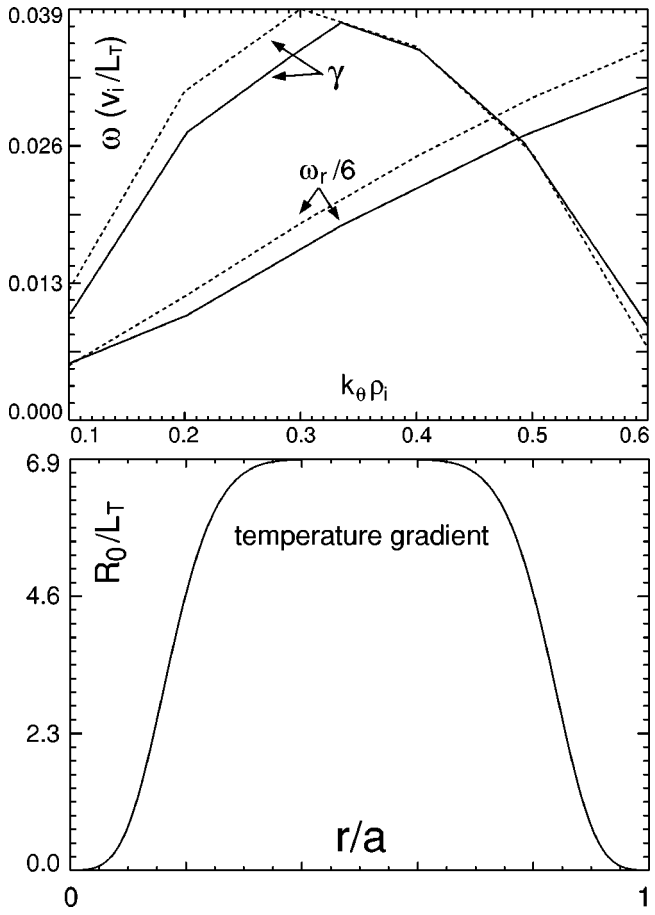

FIG. 1. Linear ITG real frequency ω_r and growth rate γ versus poloidal wave vector from GTC (solid) and FULL (dotted) calculations (upper panel), and radial profile of temperature gradients (lower panel).

consists of 32 toroidal grids (equivalent to 45 parallel grids for $q=1.4$), and a set of unstructured radial and poloidal grids with a perpendicular grid size of ρ_i. Parallel nonlinearity is neglected and a partially linearized δf method[23] is used for comparisons with the flux-tube simulations.[13]

In the upper panel of Fig. 1, the ITG real frequencies and growth rates from global GTC simulations, are compared to local calculations using a comprehensive linear eigenvalue FULL code.[24,13] The maximum linear growth rate γ from both codes agrees quite well with $\gamma=0.038v_i/L_T$, where $v_i=\sqrt{T_i/m_i}$ and m_i is the ion mass. Both the real frequency and growth rate of low k_θ modes from GTC are about 10% lower than those from FULL. Note that the maximum growth rate in current studies is about 17% lower than that in our previous studies[7] which used a tokamak geometry with finite aspect ratio corrections. Specifically, in the straight field-line magnetic coordinates (ψ,θ,ζ) with a flux function ψ, a magnetic poloidal angle θ and a toroidal angle ζ, current studies use the so-called "$s-\alpha$" model with $\zeta_0=\zeta$ and $\theta_0=\theta$ for comparisons with earlier flux-tube simulations,[13] where the metric poloidal angle is θ_0 and the metric toroidal angle is ζ_0. In our previous studies,[7] finite aspect ratio corrections were taken into account with the definitions $\zeta=\zeta_0$, $\theta=\theta_0-\epsilon\sin(\theta_0)$, and a magnetic field magnitude $B=1/[1+\epsilon\cos(\theta_0)]$, where $\epsilon=r/R_0$.

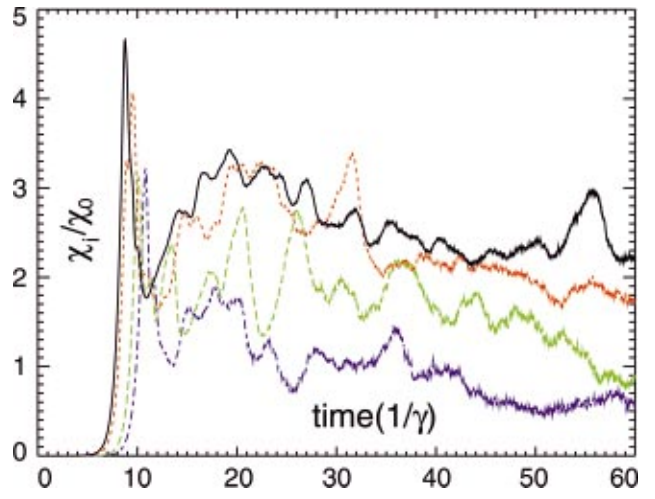

FIG. 2. (Color) Time history of ion heat conductivity χ_i in nonlinear simulations for $a/\rho_i=750$ (solid black), 500 (dotted red), 250 (dashed green), and 125 (dotted–dashed blue). In the gyro-Bohm regime, $\chi_i\simeq 2.5\chi_0$.

In nonlinear simulations, the size of the tokamak is varied such that $a/\rho_i=125$, 250, 500, and 750 with other dimensionless parameters fixed. Each of these simulations starts with very small random fluctuations which grow exponentially because of the toroidal ITG instability. Zonal flows are then generated through modulational instability[25,26] and saturate the ITG eigenmode through random shearing.[27] Finally, the nonlinear coupling of ITG-zonal flows leads to a fully developed turbulence that is insensitive to initial conditions. Shown in Fig. 2 are the time traces for the local heat conductivity χ_i measured at $r=0.5a$ and averaged over a domain of one-fifth of the simulation volume. The gyro-Bohm unit for the heat conductivity is defined as $\chi_0=\rho^*\chi_B$. Here, $\rho^*=\rho_i/a$, and the Bohm coefficient is $\chi_B=cT_e/eB$, where c,e are, respectively, the speed of light and electric charge of the electron. We observe that χ_i deviates significantly from the gyro-Bohm scaling for $a/\rho_i=125$ and 250, but reaches the gyro-Bohm scaling for $a/\rho_i=500$ and 750 with a gyro-Bohm value of $\chi_i\simeq 2.5\chi_0$. The gyro-Bohm value is about 26% below that of our previous study[7] which used a slightly different geometry as discussed above. In the present simulations with zonal flows included, the plasma is far away from the linear marginality. In fact, the linear growth rate $\gamma\simeq\omega_r/3$ for the linearly most unstable mode with $k_\theta\rho_i\simeq 0.35$. Pressure profile are kept fixed throughout the simulations using an effective collision operator for energy diffusion to model a heat bath as discussed below. Therefore, the Bohm-like scaling for small device sizes observed in our simulations is not due to a proximity to marginality or profile relaxation.

The heat conductivity from global simulations in the large device limit, $\chi_{global}=2.5\chi_0$, is compared to $\chi_{tube}=1.9\chi_0$, that of flux-tube simulations.[13] Note that there are some differences between global and local simulations in terms of geometry. Plasma parameters such as $q,\hat{s},\epsilon$ are constant in flux-tube simulations, but are functions of minor radius in global simulations. The radial box size in flux-tube simulations is $128\rho_i$, much smaller than that in global simu-

lations. Flux-tube simulations use periodic boundary conditions in the radial direction, while global simulations use fixed radial boundary conditions.

The simulation time shown in Fig. 2 is much longer than the ITG turbulence characteristic time (e.g., linear growth time or nonlinear decorrelation time), and longer than the cyclone flux-tube simulations to which several turbulence codes were benchmarked.[13] On such a long time scale, profile relaxation in full torus simulations can drive the system toward marginality. To prevent this relaxation, we use an effective collision operator for energy diffusion to model a heat bath: $\delta f_c = f_M[(v/v_i)^2 - 3/2]\delta T/T_i$, where f_M is the Maxwellian and δT is the ion temperature perturbation averaged on the flux-surface and over a minor radius range of one-fifth of the simulation domain, which is much longer than the turbulence correlation length. Ion temperatures are restored to their initial value using this heat source/sink. The effective collision time of this operator is on the order of ion energy confinement time, which is much longer than the turbulence decorrelation time. It should be pointed out that such heat source/sink, similar to that used in other global codes, is not derived from first-principles and its effects on long time simulations has not been carefully studied.

In the absence of the heat source/sink, the turbulence state could change on a time scale of profile relaxation τ_R, which is much shorter than the energy confinement time τ_E. Specifically, using the random walk argument for the diffusive transport, we can estimate

$$\tau_E \sim L_T^2/\chi_i .$$

For the case of $a/\rho_i = 500$ with measured $\chi_i = 2.5\chi_0$, $\tau_E \sim 1500/\gamma$, which is much longer than the simulation time. To estimate the profile relaxation time τ_R, we observe that in the absence of the heat source/sink, the ion heat conductivity would diminish if the temperature gradient drops from the equilibrium value T_i/L_T with $L_T = R_0/6.9$, to a nonlinear threshold of T_i/L_{NL} with $L_{NL} = R_0/6.0$ given by flux-tube simulations.[13] This profile relaxation time is

$$\tau_R \sim (L_{NL} - L_T)^2/\chi_i ,$$

when $L_{NL} - L_T \ll L_T$. For the case of $a/\rho_i = 500$ with measured $\chi_i = 2.5\chi_0$, $\tau_R \sim 34/\gamma$, which is shorter than the simulation time shown in Fig. 2. Therefore turbulence and transport would evolve on a time scale of τ_R ($\sim 34/\gamma$ for the case of $a/\rho_i = 500$) due to the profile evolution, and χ_i in long time simulations could, in principle, depend on the particular form of the heat source/sink.

Another issue for such a long time δf simulation is that the deviation of distribution function from the equilibrium, thus the discrete particle noise, grows without bound in the collisionless simulations. The issue of particle noise and conservation properties in the gyrokinetic particle-in-cell simulations has been extensively discussed.[13,28–33] In particular, a "thermostatted δf" simulation enforces a statistical steady state using a numerical dissipation.[29] A problem with this approach is that the transport level depends on the strength of this numerical dissipation.[29] We note that the velocity space sub-grid dissipation in continuum codes represents a similar numerical dissipation, which is absent in our current studies. Since turbulent transport is a stochastic process, observable quantities such as χ_i can only be obtained through ensemble averaging. Unlike linear simulations, which are time-reversible, nonlinear simulations are time-irreversible due to random round-off errors. For example, multiple simulations with the same initial condition would have different time traces for χ_i. We have done several such simulations and have observed a consistent trend in the transition of the transport scaling. However, an ensemble averaging of χ_i would require many simulations that are computationally prohibitive. All the χ_i quoted in this paper are obtained from time averaging as a proxy to the ensemble averaging.

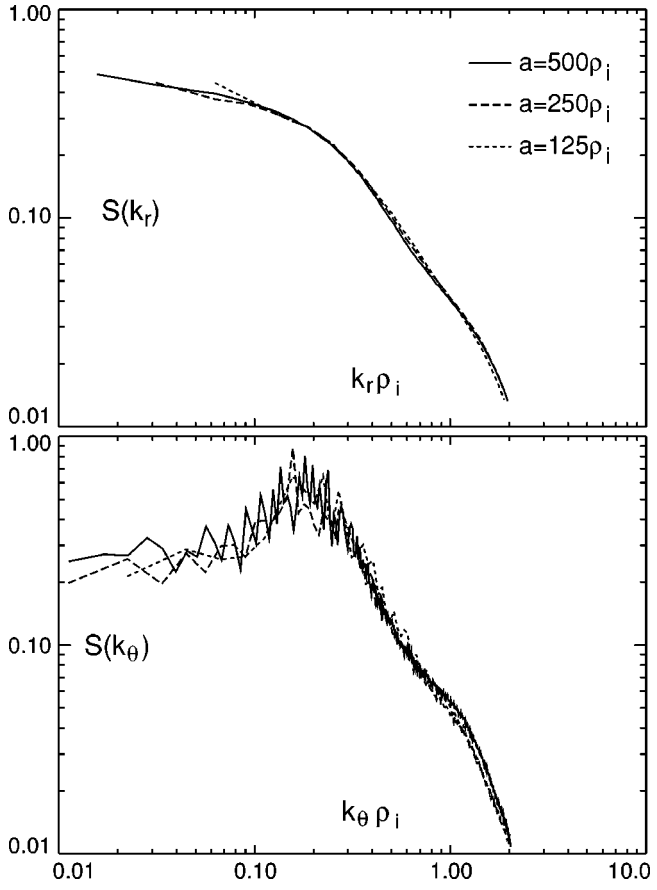

FIG. 3. Radial (k_r, upper panel) and poloidal (k_θ, lower panel) power spectra for density fluctuations for $a/\rho_i = 500$ (solid), 250 (dashed), and 125 (dotted).

III. FLUCTUATION CHARACTERISTICS

In order to understand why the transport scaling is not gyro-Bohm for $a/\rho_i \leqslant 500$, we examine the fluctuation characteristics of the ITG turbulence. The fluctuations in the quasi steady state are nearly isotropic in radial and poloidal directions because of the zonal flow shearing effects.[16,34] We measured the radial spectrum of density fluctuations at $\theta = 0$ and the poloidal spectrum at $r = 0.5a$, averaged over the toroidal angle and over several eddy turnover times after the nonlinear saturation. Both radial and poloidal spectra, as shown in Fig. 3, are independent of the device size. The

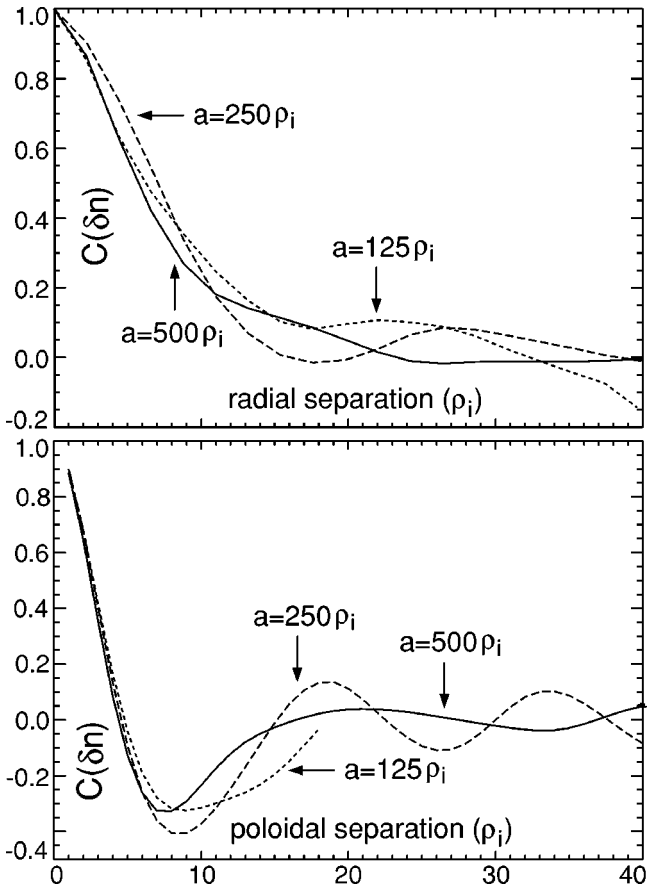

FIG. 4. Radial (upper panel) and poloidal (lower panel) correlation functions for density perturbations.

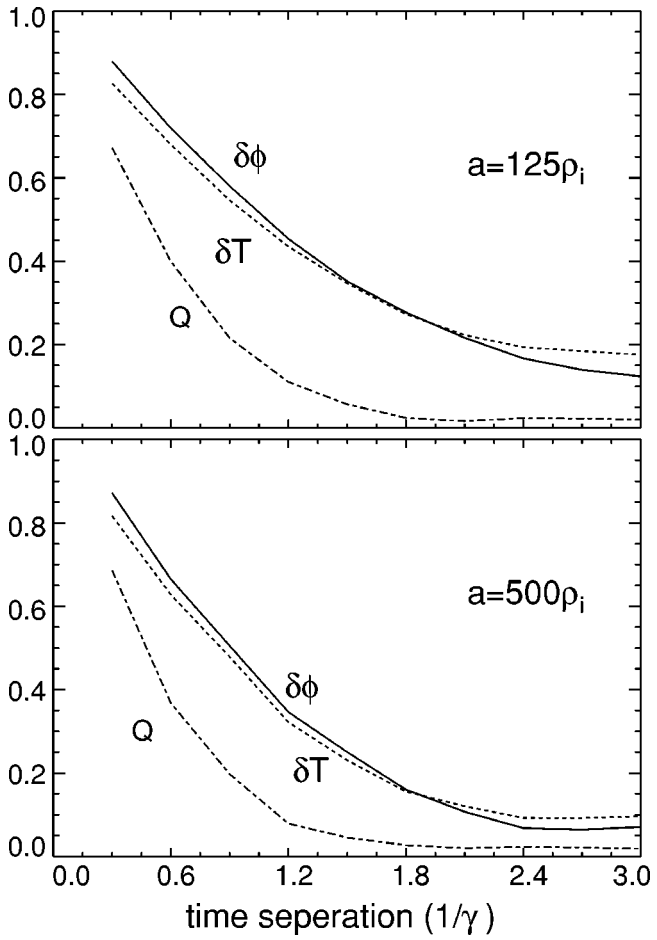

FIG. 5. Time correlation functions for electrostatic potential $\delta\phi$ (or density, solid) and temperature δT (dotted) perturbations, and heat fluxes Q (dotted–dashed).

poloidal spectra peaks at $k_\theta\rho_i \simeq 0.15$, compared to the fastest linear mode of $k_\theta\rho_i \simeq 0.35$. The energy containing part of the radial spectra is $k_r\rho_i \leqslant 0.2$.

The fluctuation spectra are consistent with two-point spatial correlation functions shown in Fig. 4. Here the radial correlation functions for field-line averaged fluctuation quantities (density perturbations, etc.) are calculated at poloidal angle $\theta=0$ using a radial location $r=0.5a$ as the reference position, and the poloidal correlations are calculated at $r=0.5a$ using $\theta=0$ as the reference position. Both radial and poloidal correlation functions are averaged in the toroidal direction because of axisymmetry and over many eddy turnover times after the nonlinear saturation assuming a statistically steady state. The correlation functions for density perturbations (or electrostatic potentials excluding zonal flow components) are found to be self-similar for different tokamak sizes, and suggest a turbulence eddy size of $\Delta r \sim 7\rho_i$ in the radial direction, which is independent of the device size. The poloidal correlation functions show some wave-like structures, indicating a partial survival of the linear dispersion. Correlation functions for temperature perturbations are similar to that of density perturbations, and correlation functions for heat fluxes show a correlation length about half of those for density (or electrostatic potential) and temperature perturbations, as expected since heat fluxes are proportional to the product of the potential and temperature fluctuations with a finite phase-shift. All correlation functions decay exponentially and no significant tails at large radial separations exist. We conclude that the fluctuation scale length is microscopic, i.e., on the order of ion gyroradius and independent of the device size.

The time correlation functions, shown in Fig. 5, are measured at $r=0.5a$ and $\theta=0$ on a rotating frame which has a velocity equal to the sum of zonal flows and diamagnetic flows, and averaged in the toroidal direction and over many eddy turnover times after the nonlinear saturation. The correlation time for the electrostatic potential (or density) and temperature is close to that of the linear growth time, $\tau_c \sim 1/\gamma$, as expected from the balance between linear growth and nonlinear decorrelation for the saturation of the instability. The correlation time for heat fluxes is about half that for the potential and temperature perturbations. The difference between two device sizes (i.e., $a/\rho_i=125$ and 500) is small. Although there are small tails in the correlation functions for the potential and temperature perturbations, these long time structures do not drive much transport, as is evident in the correlation functions for heat fluxes which decay much faster and diminish at a time separation larger than $1/\gamma$.

Both spatial and temporal correlation functions indicate that the fluctuations are microscopic in space and local in time. To further test whether large events dominate transport,

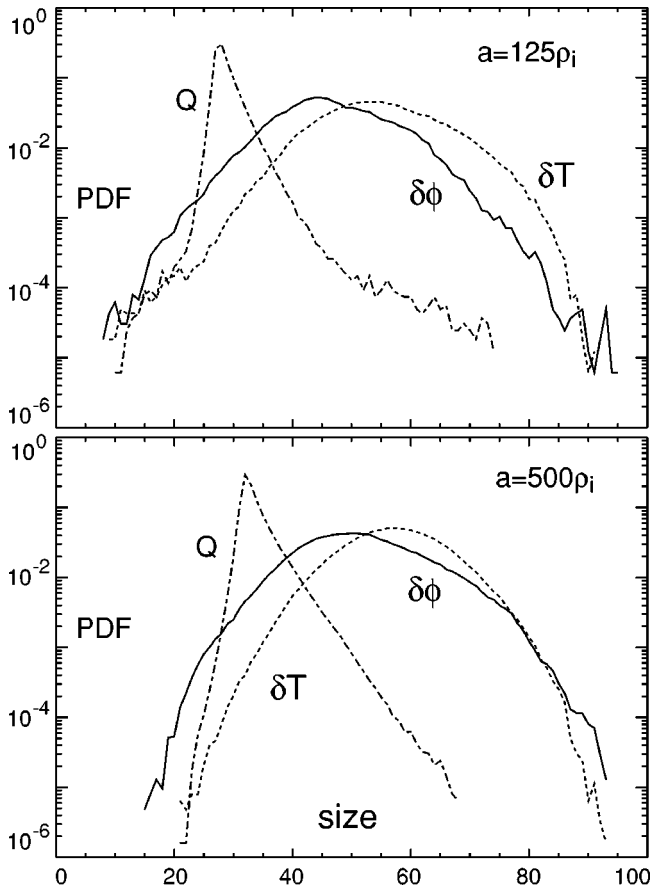

FIG. 6. Probability density functions (PDF) for electrostatic potential $\delta\phi$ (or density, solid) and temperature δT (dotted) perturbations, and heat fluxes Q (dotted–dashed).

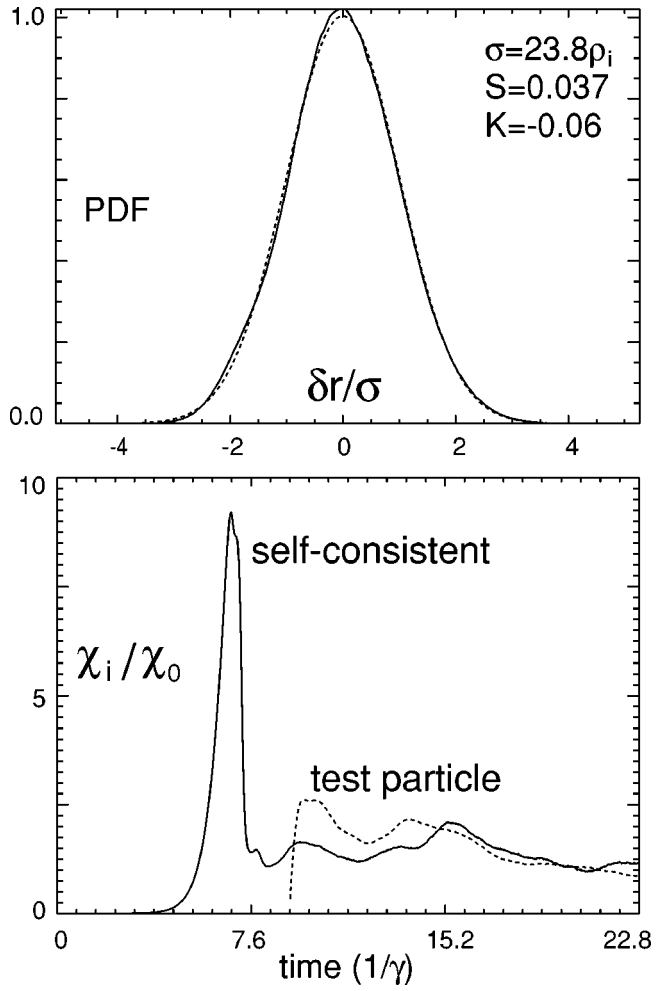

FIG. 7. Probability density functions (PDF) of test particle radial displacement δr (solid, the dotted line is a Gaussian) (upper panel), and time history of heat conductivities χ_i (lower panel).

we examine the probability distribution functions (PDF) of the potential and temperature fluctuations, and heat fluxes. These quantities are discretized in both time and space, then grouped into 100 bins according to their relative amplitudes. The counts of each bin are plotted as the PDF in Fig. 6. The maxima in Fig. 6 correspond to zeros for potential and temperature fluctuations and heat fluxes. The unit for both the size and the PDF is arbitrary. Both pointwise PDFs for potential and temperature fluctuations are close to a Gaussian with negligible tails, while the PDF for heat fluxes is a folded Gaussian[36] resulting from the folding of two correlated Gaussians (i.e., potential and temperature PDFs). These probability distribution functions for the electrostatic potential and temperature fluctuations, and heat fluxes all decay exponentially with no significant tails. This is specially true for large devices where the transport scaling is gyro-Bohm, and where there are a large number of data samplings for adequate statistics.

We further examine whether the transport is diffusive using the probability distribution function for the radial diffusion of test particles (passive particles that do not affect the turbulence). After the nonlinear saturation, at time t_0, 6 million test particles are initiated around $r(t_0)=0.5a$ with a uniform poloidal distribution. The radial displacement $\delta r(t)$ of each test particle at a later time, $t=t_0+\tau$, is defined as $\delta r(t)=r(t)-r(t_0)$. The probability distribution function (PDF) for the radial displacement $\delta r(t)$ after a few eddy turnover times, shown in the upper panel of Fig. 7, is found to be very close to a Gaussian.[7] The PDF of the Lagrangian velocity fluctuations, which resembles the step size PDF of these dispersing particles, should also approach a Gaussian after a few eddy turnover times, and therefore indicates a diffusive process.[35] Similar results have also been obtained in a Hasegawa–Wakatani turbulence.[36] Further examination of the deviation from the Gaussian reveals no singular structure in either the pitch angle or energy space. This indicates that there is no sharp resonance in the wave–particle interactions. Since the radial motion of test particles is diffusive rather than ballistic, the wave does not trap or convect the particles, but only scatters particle orbits. We can then calculate the ion heat conductivity based on the random walk model for test particle heat fluxes, $Q=-\int \frac{1}{2}v^2 D\partial f/\partial r d^3v$, using the energy-dependent diffusivity $D=\sigma^2/2\tau$, where σ is the standard deviation for the radial displacement at the time τ after the initiation of test particles. We also measure the self-consistent heat fluxes, $Q=\int \frac{1}{2}v^2\delta v_{E\times B}\delta f d^3v$, where v is the particle velocity, δf is the perturbed distribution function, and $\delta v_{E\times B}$ is the radial component of the gyrophase-

averaged $E\times B$ drifts. We found that the test particle heat fluxes are very close to the self-consistent heat fluxes. This suggests that wave transport, where the wave extracts energy from ions in the hot region and deposits it back to ions in the cold region, does not play a significant role. Thus, heat fluxes are carried by the radial diffusion of particles. Large transport events, where heat pulses propagate ballistically, are absent over this simulation time. The simulation presented in Fig. 7 used $a/\rho_i=160$ and a radial profile of the temperature gradients narrower than that shown in the lower panel of Fig. 1.

In summary, our global gyrokinetic simulations of toroidal ITG turbulence show that fluctuations are microscopic and local, that transport is diffusive, whereas transport can deviate from gyro-Bohm scaling. These results are consistent with recent dimensionless scaling studies on the DIII-D tokamak which found that ion transport and energy confinement time exhibit Bohm-like behavior while fluctuation characteristics suggest a gyro-Bohm scaling.[4] As we increase the device size further, there is a gradual transition from Bohm-like scaling to gyro-Bohm scaling.[7] Interestingly, transport studies of the JET tokamak[5] and a scan of power thresholds for the formation of internal transport barriers[6] show a similar trend. These findings show that extrapolations from present-day experiments to larger devices based on mixing length rules, which have been key building blocks in most of existing transport models, can be unreliable.

IV. TURBULENCE SPREADING

Now that the fluctuation scale length is microscopic and the test particle transport is diffusive, mixing length estimate would predict that the transport scaling is gyro-Bohm. However, the local ion heat conductivity measured at $r=0.5a$, shown in Fig. 2, exhibits Bohm-like scaling for plasmas corresponding to present-day tokamak experiments even though both the turbulence eddy size and turbulence decorrelation time are independent of the device size. These contradictory pictures clearly illustrate the failure of the mixing length approach. Specifically, using the measured eddy size of $\Delta r \sim 7\rho_i$ and decorrelation time of $\tau_c \sim 1/\gamma$, mixing length rule predicts that the heat conductivity follows a gyro-Bohm scaling with

$$\chi_i \sim \frac{(\Delta r)^2}{\tau_c} \sim 4.6\chi_0,$$

which is higher than the χ_i for any device size shown in Fig. 2.

What has been missing so far in our analysis is the size scaling of fluctuation intensity, which ultimately determines the level of transport. In the mixing length approach, the dependence of transport on the intensity is implicitly built-in through the eddy turnover time which is inversely proportional to the fluctuation amplitude. The eddy turnover time is the same as the turbulence decorrelation time τ_c, which controls the level of transport in fluid turbulence. However, in plasma ITG turbulence, the turbulence decorrelation is dominated by the shearing of zonal flows,[16] which do not drive any transport. Zonal flow convections are much stronger than the fluctuating $E\times B$ drifts (excluding zonal flow components) which control the transport level. In short, the failure of the mixing length rules, which originated from the fluid turbulence, is a direct result of the fundamental differences between the fluid turbulence and the plasma turbulence.[37] Specifically, the fluctuation intensity controls both the decorrelation and transport processes in the fluid turbulence, whereas in the plasma ITG turbulence, fluctuation intensity controls the transport level and zonal flows control the decorrelation process in the lowest order of expansion based on the nonlinear time scale separation.[26,25]

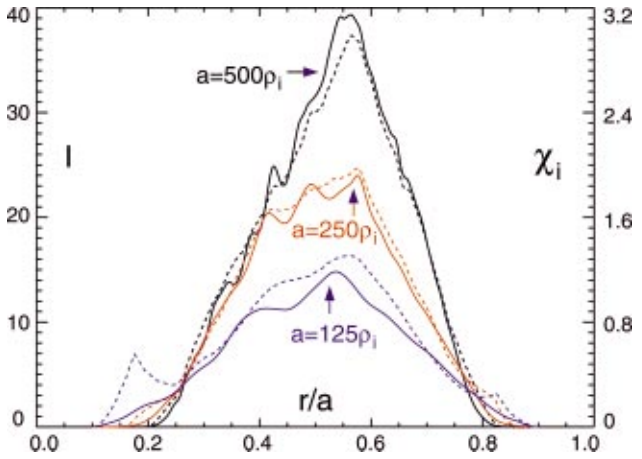

FIG. 8. (Color) Radial profiles for intensity of fluctuating potential $I=(e\delta\phi/\rho^* T_e)^2$ (solid) and ion heat conductivities χ_i/χ_0 (dotted) for $a/\rho_i=125$, 250, and 500. Note that the radial envelope of the intensity for a small device size is broader than that of a larger device size.

Therefore, in order to understand the transition of the transport scaling, we must examine the size scaling of the fluctuation intensity. Figure 8 shows the time averaged radial profiles for the fluctuation intensity (excluding zonal flow components), and the heat conductivity. Two striking features are apparent in this figure. First, the radial envelope of χ_i matches that of the fluctuation intensity I (except for a small region near the magnetic axis in the case of $a/\rho_i=125$, probably due to boundary effects). We may conclude that the transport is driven by the local fluctuation intensity. This result confirms and elaborates our earlier observation that the volume averaged χ_i is proportional to volumed averaged I.[38] Second, the device size dependence for both χ_i and I is very similar. Therefore, the transition of the size scaling for χ_i can be interpreted as the transition of the size scaling for I. Interestingly, the ratio of the heat conductivity to the turbulence intensity, both expressed in the gyro-Bohm units as shown in Fig. 8, is a constant independent on the device size and local plasma parameters, i.e., $(\chi_i/\chi_0)/(I/I_0)\simeq 0.08$, where $I_0=(T_e\rho^*/e)^2$. This points to a universality underlying the diffusive transport process.

So why does the intensity depend on device size given the fact that the fluctuations are microscopic and the transport is local? A possibility is nonlocal effects in the fluctuation intensity. If we re-plot Fig. 8 such that the area under the curve of intensity is 1, we would expect that the intensity curves for $a/\rho_i=125$, 250, and 500 lie on top of each other, if the fluctuation intensity is determined by local plasma pa-

rameters. Instead, we found that the radial envelope for a small device size is broader than that of a larger device size. This is evident in Fig. 8, which shows that, in the smaller size simulation, the intensity is lower in the center and higher toward the boundaries compared to that of a larger device simulation. We remark that even though this trend is consistent with that of linear ballooning modes, the linear eigenmode is destroyed by zonal flows[16] and should not play a dominant role in the nonlinear dynamics. Instead, a plausible mechanism for the nonlocal effects is the radial penetration of fluctuations from the unstable region to the linearly stable region. The leakage of the turbulence into the linearly stable zone has previously been observed in mode coupling analysis,[39] and global gyrokinetic simulations[40–43] of toroidal ITG turbulence. These simulations were carried out before the concept of ITG turbulence self-regulation by zonal flows[16] were generally accepted. The previous gyrokinetic simulations have not quantified the process of turbulence spreading and have not made connection between the turbulence spreading and transport scaling.

By comparing the normalized radial envelope of the fluctuation intensity as described above, it is observed that in the nonlinearly saturated phase, fluctuations spread radially toward both directions (edge and axis) for a distance on the order of $25\rho_i$ independent of the device size.[7] Using simulation parameters, a dynamical theory[9] for the turbulence spreading based on the radial diffusion predicts a spreading distance of $18\rho_i$, in rough agreement with that observed in our nonlinear simulations. If we assume that the total fluctuation energy content is not affected by this radial expansion, the fluctuation intensity scales as $(\delta\phi)^2 \propto (\delta\phi_0)^2/(1+50\rho_*)^2$, where $\delta\phi_0 = \rho^* T_e/e$ is the gyro-Bohm scaling for $\rho^* \to 0$. Since $\chi_i \propto (\delta\phi)^2$, as shown in Fig. 8, the heat conductivity should scale as $\chi_i \simeq \chi_0/(1+50\rho_*)^2$. This simple scaling formula fits well the simulation χ_i data.[7,8] The simulation results[7] for the device size, where the transition from Bohm to gyro-Bohm scaling occurs, are also in rough agreement with a theoretical prediction for the transition size of $a \simeq 420\rho_i$ using simulation parameters by a nonlinear paradigm[10] based on a radial propagation of dispersive waves, nonlinearly enhanced by drift wave-zonal flow interactions.

To elucidate the process of the turbulence spreading in the initial value calculations,[10] it is instructive to examine the dynamical evolution of radial profiles for the fluctuation intensity. In Fig. 9 is shown the time history of volume-averaged, root-mean-squared (rms) amplitude for zonal flows $v_{E\times B}$ and fluctuating potential $\delta\phi$ (excluding zonal flow components) in a GTC simulation. The linear ITG instability with a spectrum peaks near $k_\theta \rho_i \simeq 0.35$ saturates at $t \simeq 8/\gamma$ due to the shearing of nonlinearly generated zonal flows. The fluctuation amplitude then drops after the nonlinear saturation due to the reduction of amplitude of linearly most unstable modes with $k_\theta \rho_i \simeq 0.3-0.4$, but follows by a slower growth until $t \simeq 20/\gamma$ because of the increase in nonlinearly dominant modes with $k_\theta \rho_i \simeq 0.1-0.2$. The zonal flow amplitude exhibits a similar time history without any numerical instability over a period of more than 50 linear growth times.

To illustrate the radial spreading of the turbulence, we

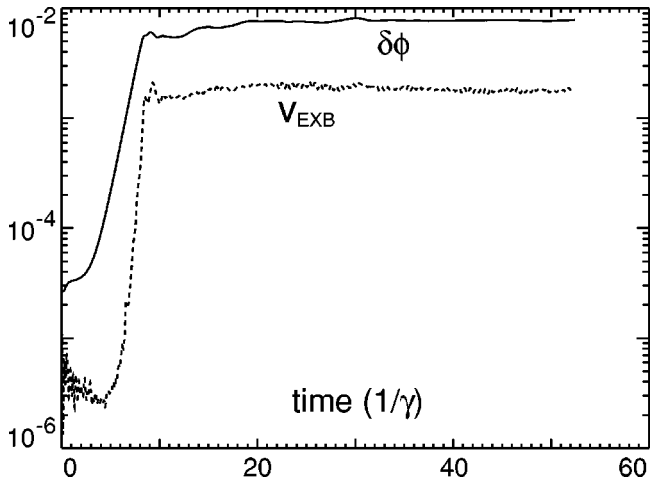

FIG. 9. Time history for amplitude of electrostatic potential $e\delta\phi/T_e$ (solid) and zonal flows $v_{E\times B}/v_i$ (dotted).

now measure the time dependence of the intensity-weighted mean location $\langle r \rangle$ and width Δr of radial envelopes for both zonal flows $v_{E\times B}$ and fluctuating potential $\delta\phi$. The most interesting time evolution occurs around nonlinear saturation, as shown in Fig. 10. In the linear phase $t < 8/\gamma$, the toroidal eigenmode $\delta\phi$ centers at $\langle r \rangle \simeq 0.43a$, where the

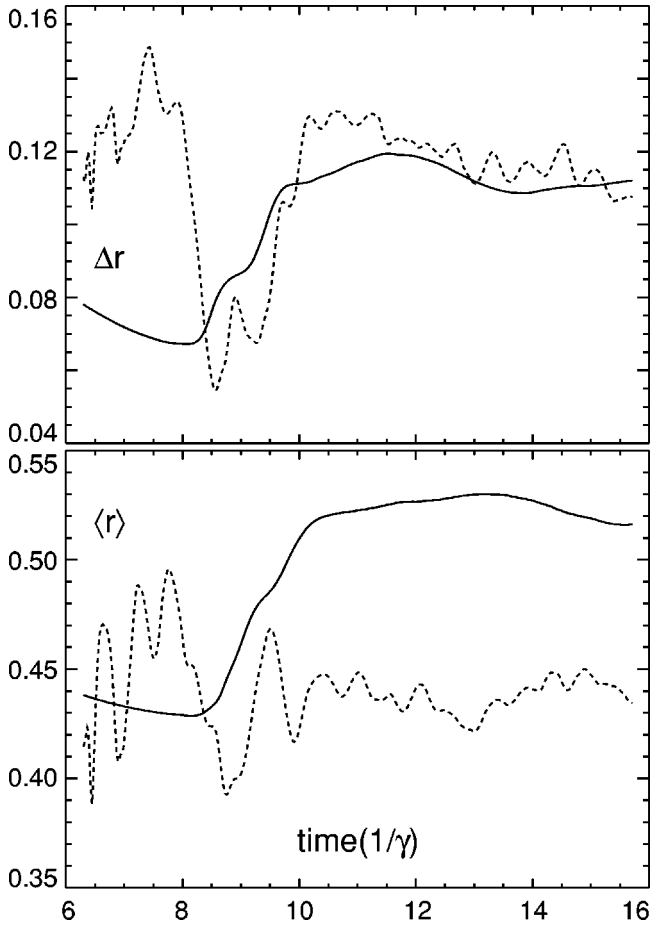

FIG. 10. Time history for the radial width $\Delta r/a$ (upper panel) and mean radial location $\langle r \rangle/a$ (lower panel) for electrostatic potential $\delta\phi$ (solid) and zonal flows $v_{E\times B}$ (dotted).

magnetic shear is lower than that at $r=0.5a$, at which the temperature gradient peaks. The mode is highly narrow with a radial width of $\Delta r \simeq 0.065a$. The width of zonal flows at this time is not of interest since it is dominated by the initial noise. At the nonlinear saturation $t \simeq 8/\gamma$, zonal flows are generated and reach the highest amplitude at $t \simeq 8.5/\gamma$ with a narrow radial width of $\Delta r \simeq 0.055a$. Within two linear growth times after the nonlinear saturation, the widths of radial envelopes for both fluctuations and zonal flows increase to $\Delta r \simeq 0.12a$, and the mean location of the fluctuations moves outward to $\langle r \rangle \simeq 0.52a$. At $t \simeq 12/\gamma$, both the radial widths and mean locations reach steady state values and remain constant through out the simulations. The expansion of the radial width for the fluctuations slightly precedes that for the zonal flows. The process of the envelope expansion shown in Fig. 10 is similar to that predicted, using simulation parameters, from a dynamical theory[10] for the radial propagation of the dispersive waves. If we call the initial radial domain in the linear phase as a linearly active zone, this envelope expansion suggests that turbulence spreads from the linearly active zone into linearly inactive zone after the nonlinear saturation.

We remark that the radial profile of χ_i, shown in Fig. 8, indicates that the divergence of radial heat fluxes is not zero, which eventually leads to a profile relaxation, i.e., a decrease of the temperature gradient in the unstable region with $R_0/L_T > 6.0$ and an increase of the temperature gradient in the stable regime with $R_0/L_T < 6.0$ as shown in the lower panel of Fig. 1. The model of a quasi-steady turbulence driven by a fixed pressure profile in our study is appropriate only on the turbulence time scale. On a longer time scale, turbulence transport will cause the pressure profile to evolve, which will influence the dynamics of turbulence spreading. A paradigm of flux-driven turbulence[44] is more appropriate for studying this regime of long time behaviors. Fully kinetic, global simulations of the flux-driven turbulence in a large tokamak on a long time scale is now computationally prohibitive, but could be addressed in future studies. However, we should point out that our current model is of practical interest since experimentally measured pressure profiles often exhibit radially localized unstable and stable domains.

V. CONCLUSION

Full torus gyrokinetic simulations of toroidal ITG turbulence found that transport scaling can deviate from gyro-Bohm even when fluctuations are microscopic and transport is local. A possible resolution to this apparent contradiction is identified as turbulence spreading from the linearly active region to the linearly inactive region in the presence of radial variation of pressure gradients. We found that fluctuations are microscopic, and that the transport process is diffusive and local, whereas the fluctuation intensity is determined by nonlocal effects. Specifically, spatial and temporal correlation functions, and radial and poloidal spectra of density fluctuations are independent of the device size. Probability density functions (PDF) of fluctuations and heat fluxes decay exponentially. Test particle transport is diffusive, and the transport coefficient is proportional to the local intensity of fluctuations. On the other hand, fluctuations are found to spread from the linearly active region to the linearly inactive region. This turbulence spreading reduces the fluctuation intensity in the unstable region, especially for the smaller device size, and thus introduces a nonlocal dependence in the fluctuation intensity. The device size dependence of the fluctuation intensity, in turn, is responsible for the observed gradual transition from Bohm to gyro-Bohm transport scaling in the presence of microscopic fluctuations. Our findings show that extrapolations from present-day experiments to larger devices based on mixing length rules, which have been key building blocks in most of existing transport models, can be unreliable.

ACKNOWLEDGMENTS

The data from FULL code calculations shown in Fig. 1 were provided by G. Rewoldt. We acknowledge helpful discussions with L. Chen, P. H. Diamond, S. Ethier, K. Itoh, S.-I. Itoh, W. W. Lee, J. Lewandowski, G. Rewoldt, W. M. Tang, W. X. Wang, R. B. White, and F. Zonca.

This work is supported by Department of Energy (DOE) Cooperative Agreement No. DE-FC02-03ER54695 (UCI), DOE Contract No. DE-AC02-76CH03073 (PPPL), and in part by the DOE SciDAC plasma microturbulence project. Simulations were performed using a massively parallel IBM SP computer at the National Energy Research Supercomputer Center (NERSC).

[1] W. M. Tang, Nucl. Fusion **18**, 1089 (1978).
[2] W. Horton, Rev. Mod. Phys. **71**, 735 (1999).
[3] J. W. Connor and J. B. Taylor, Nucl. Fusion **17**, 1047 (1979).
[4] G. McKee *et al.*, Nucl. Fusion **41**, 1235 (2001).
[5] R. V. Budny, D. R. Ernst, T. S. Hahm *et al.*, Phys. Plasmas **7**, 5038 (2000).
[6] G. T. Hoang *et al.* (private communication); "Additional heating power required for ITB formation in tokamaks," in *Proceedings of the 29th EPS Conference on Plasma Physics and Controlled Fusion*, Montreux, Switzerland, 2002.
[7] Z. Lin, S. Ethier, T. S. Hahm, and W. M. Tang, Phys. Rev. Lett. **88**, 195004 (2002).
[8] Z. Lin *et al.*, in *Proceedings of the 19th International Conference on Plasma Physics and Controlled Nuclear Fusion Research*, Lyon, France, October 2002 (International Atomic Energy Agency, Vienna, Austria, 2003), Paper IAEA-CN-77/TH/1-1.
[9] T. S. Hahm, P. H. Diamond, Z. Lin, K. Itoh, and S.-I. Itoh, "Turbulent spreading into linearly stable zone and transport scaling," to appear in Plasma Phys. Controlled Fusion.
[10] L. Chen, R. B. White, and F. Zonca, "Zonal flow dynamics and size-scaling of anomalous transport," Phys. Rev. Lett. (submitted); F. Zonca, R. B. White, and L. Chen, "Non-linear paradigm for drift wave–zonal flow interplay: Coherence, chaos and turbulence," Phys. Plasmas (to be published).
[11] E. J. Kim *et al.*, Nucl. Fusion **43**, 961 (2003).
[12] M. Yagi *et al.*, "Convective cell dynamics of drift wave turbulence," Plasma Phys. Controlled Fusion (to be published).
[13] A. M. Dimits, G. Bateman, M. A. Beer *et al.*, Phys. Plasmas **7**, 969 (2000).
[14] J. Candy and R. E. Waltz, General Atomics Report GA-A24138, 2002; Phys. Rev. Lett. **91**, 045001 (2003).
[15] J. Candy and R. E. Waltz, in "Steps toward resolving the global code controversy on broken gyro-Bohm scaling," June 2003; W. Nevins, "GYRO/GTC comparisons," presented at the Plasma Microturbulence Project Workshop, San Diego, August 2003.
[16] Z. Lin *et al.*, Science **281**, 1835 (1998).
[17] A. H. Boozer, Phys. Fluids **24**, 1999 (1981).
[18] R. B. White and M. S. Chance, Phys. Fluids **27**, 2455 (1984).
[19] Z. Lin and W. W. Lee, Phys. Rev. E **52**, 5646 (1995); Z. Lin, T. S. Hahm, W. W. Lee, W. M. Tang, and R. B. White, Phys. Plasmas **7**, 1857 (2000).

[20]W. W. Lee, Phys. Fluids **26**, 556 (1983); J. Comput. Phys. **72**, 243 (1987).
[21]T. S. Hahm, Phys. Fluids **31**, 2670 (1988).
[22]A. Brizard, J. Plasma Phys. **41**, 541 (1989).
[23]A. M. Dimits, Ph.D. thesis, Princeton University, 1988.
[24]G. Rewoldt, W. M. Tang, and M. S. Chance, Phys. Fluids **25**, 480 (1982); G. Rewoldt, W. M. Tang, and R. J. Hastie, *ibid.* **30**, 807 (1987).
[25]P. H. Diamond *et al.*, in *Proceedings of the 17th International Conference on Controlled Fusion and Plasma Physics*, Yokahama, Japan, October 1998 (International Atomic Energy Agency, Vienna, Austria, 1999).
[26]L. Chen, Z. Lin, and R. White, Phys. Plasmas **7**, 3129 (2000).
[27]T. S. Hahm, M. A. Beer, Z. Lin, G. W. Hammett, W. W. Lee, and W. M. Tang, Phys. Plasmas **6**, 922 (1999).
[28]W. W. Lee and W. M. Tang, Phys. Fluids **31**, 612 (1988).
[29]J. A. Krommes, Phys. Plasmas **6**, 1477 (1999).
[30]S. Brunner, E. Valeo, and J. A. Krommes, Phys. Plasmas **6**, 4504 (1999).
[31]R. Hatzky, T. M. Tran, A. Könies, R. Kleiber, and S. J. Allfrey, Phys. Plasmas **9**, 898 (2002).
[32]L. Villard *et al.*, Paper IAEA-CN-77/TH/1-3, in *Proceedings of the 19th International Conference on Plasma Physics and Controlled Nuclear Fusion Research*, Lyon, France, October 2002 (International Atomic Energy Agency, Vienna, Austria, 2003).
[33]Y. Idomura *et al.*, Nucl. Fusion **43**, 234 (2003).
[34]T. S. Hahm *et al.*, Plasma Phys. Controlled Fusion **42**, A205 (2000).
[35]C. Pasquero *et al.*, J. Fluid Mech. **439**, 279 (2001).
[36]R. Basu, T. Jessen, V. Naulin, and J. Juul Rasmussen, Phys. Plasmas **10**, 2696 (2003).
[37]A. Yoshizawa, S.-I. Itoh, and K. Itoh, *Plasma and Fluid Turbulence* (Institute of Physics, Bristol, 2003).
[38]Z. Lin, T. S. Hahm, W. W. Lee, W. M. Tang, and P. H. Diamond, Phys. Rev. Lett. **83**, 3645 (1999).
[39]X. Garbet *et al.*, Nucl. Fusion **34**, 963 (1994).
[40]R. D. Sydora *et al.*, Plasma Phys. Controlled Fusion **38**, A281 (1996).
[41]S. E. Parker, H. E. Mynick, M. Artun *et al.*, Phys. Plasmas **3**, 1959 (1996).
[42]Y. Kishimoto, T. Tajima, W. Horton, M. J. LeBrun, and J. Y. Kim, Phys. Plasmas **3**, 1289 (1996).
[43]W. W. Lee and R. Santoro, Phys. Plasmas **4**, 169 (1997).
[44]M. Ottaviani and G. Manfredi, Phys. Plasmas **6**, 3267 (1999); X. Garbet *et al.*, Nucl. Fusion **39**, 2063 (1999).